Helicopter main rotor dynamics by neuro-fuzzy classification with bred vector

Ivana Y. Sumida[a] [1], Haroldo F. de Campos Velho [b] and Thiago G. Ritto[c]

[a]Flight Test Research Institute - Aerospace Technology and Science Department, São José dos Campos, SP, Brazil

[b]Associated Laboratory for Computing and Applied Mathematics - National Institute for Space Research, São José dos Campos, SP, Brazil

[c]Department of Mechanical Engineering - Federal University of Rio de Janeiro, Rio de Janeiro, RJ, Brazil

Abstract

Helicopters are aricraft with rotational wings with many sub-systems presenting nonlinear dynamics. One of these sub-systems is the main rotor, which is responsible to provide the sustentation of the aircraft. Nonlinear equations of motion are applied to simulate the dynamics of the main rotor. The main rotor responses are analyzed carrying out some simulations with different numerical values of frequency associated to the motion equations. The helicopter dynamics can presents a very dangerous situation, such as the ground resonance caused by the interaction between the ground and the rotorcraft. The rotor dynamical analysis is performed by breeding technique, where the model is executed under a perturbed initial condition. The difference between the reference and the perturbed dynamics is called bred vector. The time series of bred vector magnitude is employed for describing classes of dynamics predictability, in other words, the classes represent the degree of confidence for the simulated dynamics. Two neuro-fuzzy classifiers are used in our analysis: ANFIS and Guaje software packages. ANFIS codify the Takige-Sugeno approach, while Gauje is a computer system dealing with Mamdami formulation.

Keywords: Dynamic analysis, helicopter flight dynamics, bred vector, neuro-fuzzy systems.

1. Introduction

Helicopter main rotor dynamics can be represented by a set of nonlinear equations. A particular vibration on the main rotor is produced while the helicopter is on the ground over its landing gear. This instability is known as ground resonance and it has been studied since 1958 by Coleman and Feingold [1, 2].

[1]E-mail Corresponding Author: ivanayoshie@yahoo.com.br

The study of the helicopter dynamical system is important to identify different types of the aircraft behavior. In particular, for understanding how the behavior changes as the system parameter changes, to avoid phenomena such as the ground resonance.

The dynamical system characterization has been done using several tools such as Lyapunov exponents, bifurcation diagram, Poincaré section. An approach known as *bred vector* has been used in data assimilation and atmospheric models [5, 6]. Bred vectors are the difference between two simulations fo the dynamical system. Such diffenrece is computed from the reference dynamics (control) and perturbed dynamics, after some time-steps [8].

Here, the bredding method is used to analyze the helicopter rotor dynamics and provide pairs of input/output required for neuro-fuzzy system GUAJE (Generating Understandable and Accurate fuzzy models in a Java Environment) [17]. GUAJE is based on Mamdami's fuzzy scheme. The Mamdami's approach can provide a more easily interpretable rules. It was employed as a classifier and also for deriving some rules for the rotor dynamics. Furthermore, the accuracy results obtained with GUAJE was very good.

2. Rotor Model Dynamics

In order to obtain the governing equations of motion of a three-blade helicopter which is modeled by a simplified multibody system, the following assumptions are made: (1) the movement occurs only in (x, y) plane, (2) the blades are rigid bars, (3) the rotor head is a rigid cylinder with constant rotational speed, and (4) only the first axial/lateral modes of the helicopter are taken into account. With such hypotheses, the system has five degrees of freedom (DOF): the x and y displacements of the center of mass of the rotor head, and the blade angles β_i ($i = 1, ..., N$), where N is the number of blades, which is three in the present model. Using the mathematical model developed by the authors [6], Figure 1 shows the general scheme of the proposed model.

The blades are attached to the rotor head through a point called link, distant d from origin O, the geometric center of the rotor head. At each link, there is a linear torsional spring and damping.

Let us consider a inertial frame of reference, with basis $\{\mathbf{n}_1, \mathbf{n}_2\}$, and a Cartesian coordinate system with origin O. The position of the center of mass of the rotor head H^* with respect to the origin can be written as:

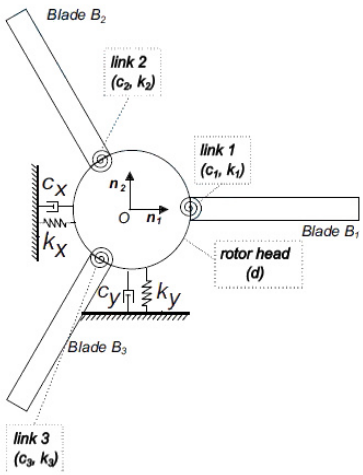

Figure 1: System Coordinate and Degrees of Freedom [6]

$$O\mathbf{r}H^*(t) = [x(t) + e\cos(\epsilon + \Omega t)]\mathbf{n}_1 + [y(t) + e\sin(\epsilon + \Omega t)]\mathbf{n}_2 \tag{1}$$

where x is the displacement of the geometric center of the rotor head in the direction of $\mathbf{n}_1$, y is the displacement of the geometric center of the rotor head in the direction of $\mathbf{n}_2$, Ω is the rotor head constant rotation speed, e is the eccentricity of the rotor head, ϵ is the angle of the eccentricity (figure 2).

Considering that each blade has a phase angle (ϕ_i), or azimuth, the position of the center of mass of the blade B_i with respect to O can be written as:

$$\begin{aligned} O\mathbf{r}B_i(t) = &[x(t) + d\cos(\phi + \Omega t) + \left(\frac{hB_i}{2}\right)\cos(\phi + \Omega t + \beta_i(t))]\mathbf{n}_1 \\ &+[y(t) + d\sin(\phi + \Omega t) + \left(\frac{hB_i}{2}\right)\sin(\phi + \Omega t + \beta_i(t))]\mathbf{n}_2 \end{aligned} \tag{2}$$

where h_{B_i} is the length of the i-th blade and β_i is the angle of the i-th blade in the direction of $\mathbf{n}_3$ with respect to a frame that rotates with the rotor head.

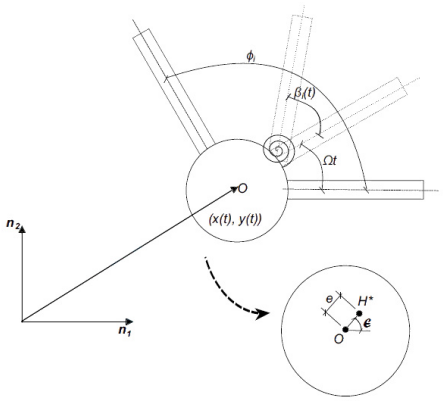

Figure 2: Blade Dynamics Scheme [6]

2.1 Newton Second Law

Applying Newton's second law (figure 3), we have:

$$\mathbf{F} = \frac{d\mathbf{G}^T}{dt} \tag{3}$$

where $\mathbf{G}^T$ is the total linear momentum of the system and the derivative is with respect to the inertial frame of reference. The vector with external forces $\mathbf{F}$ acting on the system due to the tower stiffness/damping and due to gravity are written as:

$$\mathbf{F} = [-c_x\dot{x}(t) - k_x x(t)]\mathbf{n}_1 + [-c_y\dot{y}(t) - k_y y(t) - (Nm_{B_i} + m_H)g]\mathbf{n}_2 \tag{4}$$

where g is the acceleration of gravity, k_x, k_y, c_x, c_y are the stiffness and damping coefficients related to the helicopter, in the $\mathbf{n}_1$ and $\mathbf{n}_2$ directions. The i-th blade mass is m_{B_i} , and m_H is the sum of the mass of the rotor head.

The total linear momentum is composed by the linear momentum of the rotor head plus the linear momentum of the blades. The linear momentum of the nacelle/tower is given by:

$$\mathbf{G}_H = m_H\mathbf{v}_{H*} \tag{5}$$

where $\mathbf{v}_{H*}$ is the velocity of the center of mass of the rotor head, which is the derivative of the position O_{H*} with respect to the inertial frame of reference. The linear momentum of the i-th blade is given by:

$$\mathbf{G}_{B_i} = m_{B_i}\mathbf{v}_{B_i} \tag{6}$$

where $\mathbf{v}_{B_i}$ is the velocity of the center of mass of the i-th blade, which is the derivative of the position $O\mathbf{r}B_i$ with respect to the inertial frame of reference. The total linear momentum of the system, if all blades have the same mass, is then defined by:

$$\mathbf{G}_T = \mathbf{G}_H + \sum_{n=1}^{N} \mathbf{G}_{B_i} = m_H\mathbf{v}_H * + m_B \sum_{n=1}^{N} \mathbf{v}_{B_i} \tag{7}$$

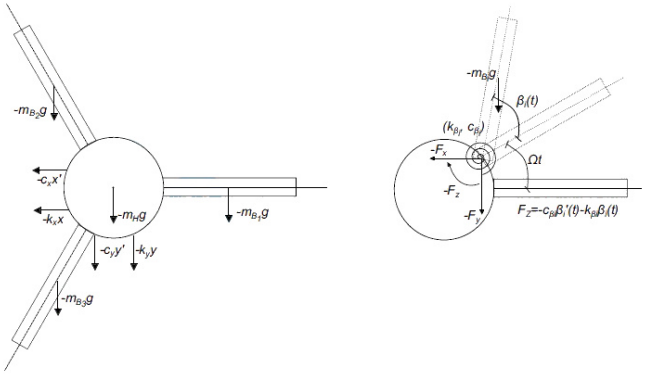

Figure 3: Acting Forces [6]

After some manipulations, we get the first two equations of motion of the system:

$$\begin{aligned}(Nm_B + m_H)\ddot{x}(t) + c_x\dot{x}(t) + k_x x(t) = em_H\Omega^2\cos(\epsilon + \Omega t) + \\ dm_B\Omega^2\sum_{n=1}^{N}\cos(\phi_i + \Omega t) + m_B\left(\frac{h_B}{2}\right)\sum_{n=1}^{N}[\ddot{\beta}_i(t)\sin(\phi_i + \Omega t + \beta_i(t)) + \\ (\Omega + \dot{\beta}_i(t))^2\cos(\phi_i + \Omega t + \beta_i(t))]\end{aligned} \tag{8}$$

$$(Nm_B + m_H)\ddot{y}(t) + c_y\dot{y}(t) + k_y y(t) + (NmB_i + m_H)g = em_H\Omega^2 \sin(\epsilon + \Omega t) + dm_B\Omega^2 \sum_{n=1}^{N} \sin(\phi_i + \Omega t) + m_B\left(\frac{h_B}{2}\right)\sum_{n=1}^{N}[-\ddot{\beta}_i(t)\cos(\phi_i + \Omega t + \beta_i(t)) + (\Omega + \dot{\beta}_i(t))^2 \sin(\phi_i + \Omega t + \beta_i(t))] \quad (9)$$

where the over dot is the derivative with respect to time.

Unfortunately, these equations are not sufficient to analyze the system because the system has $(N + 2)$ DOFs. One possibility is to develop three equations of motion for each rigid body, and end up with $3(N + 2)$ equations; but, fortunately, we do not need so many equations. Since we are not interested in the interaction forces among the rigid bodies, we will calculate the angular momentum with respect to each link, so that only N more equations are required to analyze the system. The price to pay is that the link is a moving point not coincident with the center of mass, therefore, attention is required because $\mathbf{M} \neq d\mathbf{H}/dt$.

2.2 Euler Law

Applying the Euler's law, we have:

$$\mathbf{M}_{L_i}^{B_i} = \frac{d\mathbf{I}_{L_i}^{B_i}\omega}{dt} + (m_{B_i})L_i\mathbf{r}B_i{}^* \times \mathbf{a}L_i \quad (10)$$

where $\mathbf{M}_{L_i}^{B_i}$ is the vector of external moments acting on the i-th blade with respect to link L_i. The angular inertia tensor of the i-th blade with respect to link L_i is $\mathbf{I}_{L_i}^{B_i}$, $L_i\mathbf{r}B_i$ is the position of the center of mass of the i-th blade with respect to L_i , and $\mathbf{a}L_i$ is the acceleration of L_i. Note that the additional term on the right of the above equation appears because the point L_i has an acceleration which is not zero. The vector of external moments acting on the i-blade is given by:

$$\mathbf{M}_{L_i}^{B_i} = [-c_i\dot{\beta}_i(t) - k_i\beta_i(t) - m_{B_i}g\left(\frac{h_{B_i}}{2}\right)\cos(\phi_i + \Omega(t) + \beta_i(t)]\mathbf{b}_3 \quad (11)$$

where k_i and c_i are i-th blade stiffness and damping coefficients. The position of the center of mass of the i-th blade with respect to L_i can be written as:

$$L_i rB_i(t) = \left[\left(\frac{h_{B_i}}{2}\right)\cos(\phi_i + \Omega(t) + \beta_i(t)\right]\mathbf{n}_1 + \left[\left(\frac{h_{B_i}}{2}\right)\sin(\phi_i + \Omega(t) + \beta_i(t)\right]\mathbf{n}_2 \tag{12}$$

and the acceleration of the link is given by:

$$\mathbf{a}_{L_i}(t) = [\ddot{x}(t) - d\Omega^2\cos(\phi_i + \Omega(t)]\mathbf{n}_1 + [\ddot{y}(t) - d\Omega^2\sin(\phi_i + \Omega(t)]\mathbf{n}_2\ . \tag{13}$$

Again, after some manipulations, we get the extra N equations of motion of the system ($i = 1, ..., N$):

$$\frac{1}{3}mB_i h_{B_i}^2\ddot{\beta}_i(t) + c_i\dot{\beta}_i(t) + k_i\beta_i(t) + mB_i\frac{hB_i}{2}d\Omega^2\sin\beta_i + mB_i g\frac{hB_i}{2}\cos(\phi_i + \Omega t + \beta_i(t)) = mB_i\frac{hB_i}{2}[\ddot{x}(t)\sin(\phi_i + \Omega t + \beta_i(t)) - \ddot{y}(t)\cos(\phi_i + \Omega t + \beta_i(t))] \tag{14}$$

Setting $N = 3$ (three blade system), the five equations of motion of the proposed model are given by Eqs. (8), (9) and (14), which form a set of coupled, nonlinear, second order ordinary differential equations, that must be solved numerically.

3 Non-linear analysis

An analysis to identify the dynamics behaviour was carried out using the 0-1 test [20] (red OBS: Citar o teu artigo onde esta analise foi feita!). The test is applied to detect chaos regime in a time series. Other approaches can be used to distinguish the nature of the dynamics, such as the Lyapunov exponent [18, 19]. The 0-1 test is much simpler, and it can be applied to continuous or discrete time series from experimental data or a mathematical equations. The 0-1 test returns values close to one in the presence of chaos and close zero otherwise [21].

Our results show ...

3.2 Bred vector analysis

Breeding was first used as a method to generate initial perturbations for ensemble forecasting in numerical weather prediction at the National Centers for Environmental Prediction (NCEP) [8, 9] but it was also employed in several nonlinear models [10, 13, 14, 15].

The method consists in running the nonlinear model twice. First of all, the model is run with the original data (control run) next another execution is realized with a small perturbation added to it. The control solution is subtracted from the perturbed solution after a fixed amount of time steps and the rescaled difference (a bred vector) is then added to the control run and the process repeated. The growth rate of the bred vectors is a measure of the local instability of flow [9, 13]. Figure 4 shows bred vectors growth.

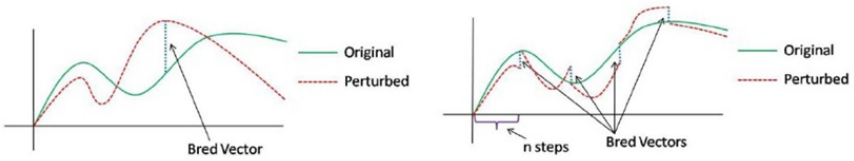

Figure 4: Bred vector growth [16]

The bred vector algorithm [11] is described in detail below:

1. Start with a initial perturbation $\delta r_0 = r_0 + \delta r_0$. The initialization is executed only once

2. Add the perturbation calculated in the previous step to the basic solution, integrate the perturbed condition with the nonlinear model for a fixed number of time steps, and subtract the original unperturbed solution from the perturbed nonlinear integration $\delta r_0(t) = \Phi(\delta r_0 + r_0, t_0 + n\Delta t) - \Phi(r_0, t_0 + n\Delta t)$

3. Evalute the growth ratio $g = \frac{1}{n} \ln \left(\frac{\|\delta r(t)\|}{\|\delta r_0\|} \right)$

4. Re-scale the perturbation, and repete the process.

Breeding method has been used with success to predict the behavior of chaotic systems such as the Lorenz strange attractor [10] and the three-waves systems [13]. It was also applied to the AGCM-CPTEC model generating bred vectors that indicate regions with high and low predictability, regions

with small and large bred vector magnitude [32]. Our objective is to extend such methodology to investigate the rotor model dynamics.

3.3 Classification: neuro-fuzzy approach

The combination of fuzzy logic and neural networks are known as neuro-fuzzy. It constitutes a hybrid intelligent system which is capable of reasoning and learning in an uncertain and imprecise environment. The idea is to integrate different approaches to solve problems, extracting the advantages from each of them.

The groundwork of the neuro-fuzzy approach is to create or improve a fuzzy system automatically by means of neural network methods. An even more important aspect is that the system should always be interpretable in terms of fuzzy if-then rules because it is based on a fuzzy system reflecting vague knowledge.

In short, we can point out, among others, some neuro-fuzzy software such as the professional commercial tools like the Matlab toolboxes which include the well-known ANFIS (Adaptive Neuro-Fuzzy System), GUAJE (Generating Understandable and Accurate Fuzzy Models in a Java Environment) and NEFCLASS (Neuro-Fuzzy Classification). In this work, the experiments have been made with ANFIS and GUAJE. However, we will present the results only with GUAJE because this takes the better results.

3.3.1 ANFIS neuro-fuzzy classifier

3.3.1 Guaje neuro-fuzzy classifier

4 Numerical Results

The computer results were conducted in an Intel Core I5 2.27 GHz under Linux operating system. Our mathematical model described in Section 2 was implemented in Matlab R2011b.

The rotor dynamical system of equations were integrated numerically using the fourth-order RungeKutta time scheme with a time step of $\Delta t = 0.0001$, Figure 5 illustrates the trajectory on space-phase which represents the movement of the rotor head, as we can see it is confined in a finite region. Finally, we set the following parameters: k_x and k_y equal to 113 lb/ft, m_{B_i} equal to 0.1 slug, m_H equal to 6.8 slugs, Ω equal to 90 rad/s and h_B equal to 10 ft.

4.1 Non-linear regime evaluation (Test 0-1)

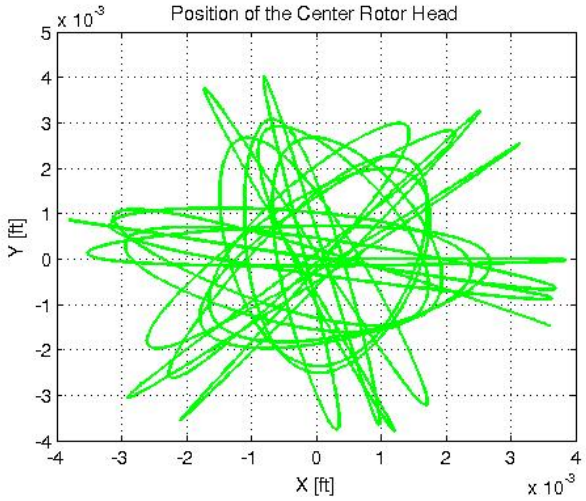

Figure 5: Position of the Center Rotor Head

We used the 0-1 test to identified if our rotor dynamics is chaotic or regular. The encoded program was developed by [27], the total size of the time series for the variable $x(t)$ is 110.000 but we choose a sample of 2000 elements. At each 50 time steps, we took one element of the time series. We set the lower bound for c equal 0 and the upper bound equal π. The asymptotic growth rate K found was -0.0113 which means that the helicopter rotor dynamics is regular.

4.3 Bred vector analysis

In this work we are interested in the study of stable dynamics, it was the reason that we set frequency Ω equal to 90 rad/s. For our analysis, we divided the system in two regimes. The first regime is identified "turn right" Figure 6(a), and the second regime "turn left", Figure 6(b). The same idea was applied in [10] with the Lorenz model they call the regimes as "warm winter" and "cold winter". Although apparently simple, in these systems it is hard to identify when a regime change.

The bred vector approach was applied in the rotor dynamics model. The first integration was done with $\Delta t = 0.0001$, and a second run started from an initial perturbation δx_0 added to the control at time t_0. The difference δx between the perturbed and the control run was taken at every 8 times steps. The growth rate of the perturbation was measured per time step as [10]:

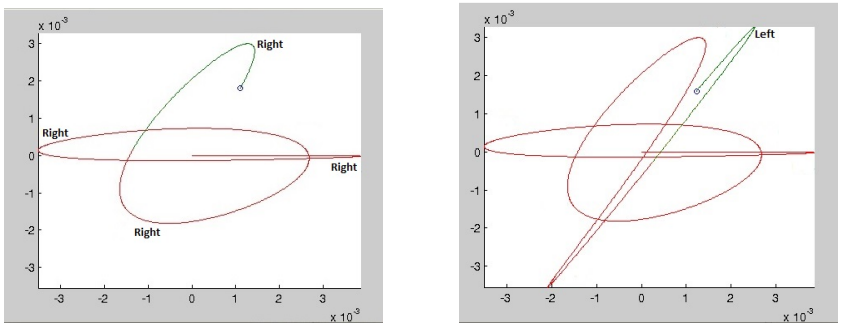

(a) Right Regime (b) Left Regime

Figure 6: Right and Left Regime

$$g = \frac{1}{n} \ln \left(\frac{\|\delta x\|}{\|\delta x_0\|} \right) \tag{15}$$

We used 6 colors to indicate the bred vector growth intervals, described in Table 1. Figure 7 illustrated the bred vector growth after 8 times steps.

Table 1: Color that Represents the Bred Vector Growth

Color	BV Growth
Yellow:	[-0,0930 ; -0,0196]
Green:	(-0,0196 ; -0,0013]
Blue:	(-0,0013 ; 0,0033]
Red:	(0,0033 ; 0,0075]
Black:	(0,0075 ; 0.0250]
Cyan:	(0,0250 ; 0,2006]

4.4 Neuro-fuzzy classification

The rotor dynamic model was then executed for 110.000 time steps. In the execution the regimes change 470 times, 365 times turn right and 105 left. From the observation of the system depicted in Figures 6(a), 6(b) and 7, the following rules were observed:

1. The presence of four or five blue stars indicates that the trajectory will turn (right or left)

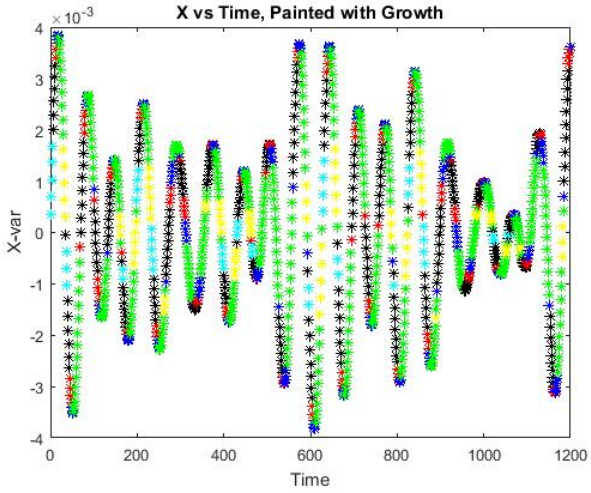

Figure 7: X(t) for Stable Dynamic ($\Omega = 90$ rad/s) with the Bred Vector Intervals.

2. After 4 cycles turning right, the trajectory will turn left one or two times on the 5th or 6th cycle

Using these rules we want to embrace mapping of different classes of dynamics. It is a little difficult work to find the rules presented above. This task requires much knowledge and time of the analyst. One way to help the analyst is to automate the rules that can characterize the dynamics. It can be done using neuro-fuzzy approach which is an appropriate artificial intelligence technique for this particular problem.

We use the GUAJE system to combine knowledge from the expert information and/or from the data. Figure 8 shows the automatic rules (17) generated by the GUAJE system. Several rules can be grouped to become even easier interpretable system.

Moreover, we use the magnitude of bred vector as the input for a presented neuro-fuzzy classifier GUAJE. Each sample is composed of the number of color stars that represents the bred vector magnitude. The start and end of each sample occurs when the start/end of a curve which corresponds the 4 or 5 blue bred vector.

For example, in Figure 9 the sample has start at A and end at B. After the blue bred vector, we started the count of each color: green (13), yellow (2), cyan (0), black (10), red (4) and blue (4). If one of the magnitudes does not appear in the sample, we attribute zero (0) for the color not found, in

Rule	Type	If Green	AND Yellow	AND Cyan	AND Black	AND Red	AND Blue	THEN Turn
1	I			0.0				1.0
2	I		3.0	1.0				0.0
3	I		4.0	1.0				1.0
4	I			2.0	8.0	3.0		1.0
5	I			2.0	9.0	3.0		0.0
6	I			2.0		4.0		0.0
7	I			3.0			4.0	1.0
8	I			3.0	6.0		5.0	1.0
9	I			3.0	7.0		5.0	1.0
10	I			3.0	8.0		5.0	0.0
11	I			3.0			6.0	0.0
12	I			4.0	6.0	3.0		1.0
13	I	10.0		4.0	6.0	4.0		1.0
14	I	11.0		4.0	6.0	4.0		0.0
15	I			4.0	6.0	5.0		0.0
16	I			4.0	7.0			0.0
17	I			5.0				0.0

Figure 8: Automatic Rules Generated by GUAJE

this example it does not show magnitude cyan.

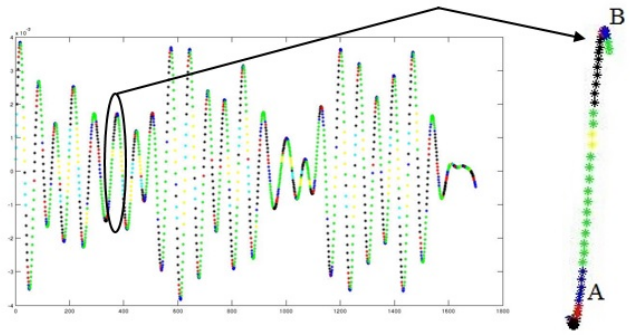

Figure 9: Input Sample for Neuro-Fuzzy System

The output was defined in Section 5.2. One output regime is "turn right" (class 1), and the other output regime is "turn left" (class 0). We have used 470 samples, divided as: training (329 - 70% of the total samples) and validation (141 - 30% of the total samples).

We have performed 4 types of experiments using the helicopter rotor dynamics. First, we divided the validation data set into balanced and unbalanced samples, then we separated in normalized and unnormalized data. Different techniques can be use to normalize the data set, in this work we used min max normalization which takes the data inputs and mapped into a range [0,1].

The confusion matrices obtained by the use of GUAJE with unbalanced set are given in Table 2. The accuracy results for the rotor dynamics using unbalanced set achieved 84.4% for unnormalized data and a little bit better for normalized data with 85.1%. The lines correspond to the real class and

the column to system response.

Table 3 bring the confusion matrices obtained by the use of GUAJE with balanced samples. The accuracy results for the rotor dynamics applying balanced set achieved 85.8% for unnormalized data. We obtained the better results with normalized data reaching 87.2%.

Table 2: Confusion Matrices - Unbalanced Data

Unnormalized			Normalized		
Class	0	1	Class	0	1
0	**22**	11	0	**22**	11
1	11	**97**	1	10	**98**

Table 3: Confusion Matrices - Balanced Data

Unnormalized			Normalized		
Class	0	1	Class	0	1
0	**67**	3	0	**66**	4
1	17	**54**	1	14	**57**

5 Final remarks

References

[1] Lee, Y.K. and Kim, K.J. Ground resonance analysis for an eight-degrees-of-freedom rotorcraft with double-stage oleo-pneumatic shock absorbers, Journal of a Aircraft, Vol 47, No. 5, pp. 65-91, 2010.

[2] Coleman, R.P. and Feingold, A.M. Theory of self-excited mechanical oscillations of helicopter rotors with hinged blades, NACA Report 1351, 1958.

[3] Lytwyn, R., Miao ,W. and Woitsch, W. Airborne and ground resonance of hingeless rotors, Journal of the American Helicopter Society, Vol 17, No. 2, pp. 2-9, 1972.

[4] Jang, J. and Chopra, I. Ground air resonance of a bearingless rotors in hover, 28^{th} Structures, Structural Dynamics and Materials Conference. Monterey, CA, U.S.A., 1987.

[5] Dzygadlo, Z. and Kowaleczko, G. Ground resonance of a helicopter, Journal of Theoretical and Applied Mechanics, Vol 1, No. 38, pp. 65-91, 2000.

[6] Gonzaga, F.G. Modelos computacionais para análise da vibração acoplada rotor-pás com aplicação em turbinas eólicas e ressonância de solo de helicópteros, Projeto de Graduação, Departamento de Engenharia Mecânica da Escola Politécnica, Universidade Federal do Rio de Janeiro, 2013.

[7] Garrison, P. How things work: ground resonance, http://www.airspacemag.com/flight-today/how-things-work-ground-resonance-94660854/?no-ist, Access in 09/20/2016, 2008.

[8] Toth, Z. and Kalnay, E. Ensemble forecasting at NCEP: the generation of perturbations, Bull. Amer. Meteor. Soc., Vol 74, pp. 2317-2330, 1993.

[9] Toth, Z. and Kalnay, E. Ensemble forecasting at NCEP and the breeding method, Monthly Weather Review, Vol 126, 1997.

[10] Evans, E., Bathi, N.K., Kinney, J., Peña, L.P.M., Yang, S-C, Kalnay, E. and Hansen, J. Rise undergraduates find that regime changes in Lorenz's model are predictable, Bull. Amer. Meteor. Soc., Vol 85, pp. 520-524, 2004.

[11] Kalnay, E. Atmospheric modeling, data assimilation and predictability, Chapter 6. Cambridge University Press, 2001.

[12] Santos, P.L.B., Sandri, S.A. and Campos Velho, H.F. Uncertainties formulated as a classification problem applied to chaotic system, Mecánica Computacional, Vol 33, pp. 1783-1791, 2014.

[13] Cintra, R.S.C. and Campos Velho, H.F. Predictability for a chaotic solar plasma system,Iberian and LatinAmerican Congress on Computational Methods for Engineering (XXIX CILAMCE), pp. 1-8, 2008.

[14] Pasini, A. External forcings and predictability in Lorenz model: An analysis via neural network modelling, IL Nuovo Cimento, Vol 31, No. 3, 2008.

[15] Wang, X. and Bishop, C.H. A comparison of breeding and ensemble transform Kalman filter ensemble forecast schemes, Jounal of the Atmospheric Sciences, Vol 60, No. 9, 2003.

[16] Santos, P.L.B. Previsibilidade em sistemas caóticos utilizando sistemas neuro-difusos, Dissertação de Mestrado, Instituto Nacional de Pesquisas Espaciais (INPE), São José dos Campos. Annuals of the New York Academy of Science, 357, 422-434, 2014.

[17] Lorenz, E. N. Deterministic non-periodic flow, Journal of the Atmospheric Sciences, Vol. 20, pp. 130141, 1963.

[18] Takens, F. Detecting strange attractors in turbulence, Dynamical Systems and Turbulence, Springer Berlin Heidelberg, Vol. 898, pp. 366-381, 1981.

[19] Wolf, A., Swift, J.B., Swinney, H.L. and Vastano, J.A. Determining Lyapunov exponents from a time series, Physica D, Vol. 16, pp. 285-317, 1985.

[20] Gottwald, G. and Melbourne, I. A new test for chaos in deterministic systems, Proceedings of the Royal Society of London A, Vol. 460, pp. 603-611, 2004.

[21] Gottwald, G. and Melbourne, I. Testing for chaos in deterministic systems with noise, Physica D, Vol. 212, pp. 100-110, 2005.

[22] Devi, P.S., Singh, S.B. and Sharma, S.A. Deterministic dynamics of the magnetosphere: results of the 01 test, Nonlinear Processes in Geophysics, Vol. 20, pp. 11-18, 2013.

[23] Litak, G. and Sawicki, J., Regular and chaotic vibrations in the rub impact model of a jeffcott rotor with a fractional restore force, Eur Phys J Appl Phys, Vol. 64, 31303, 2013.

[24] Piccirillo, V., Balthazar, J. and Tusset, A. Chaos control and impact suppression in rotor-bearing system using magnetorheological fluid, Eur Phys J Appl Phys, Vol. 224, pp. 30233040, 2015.

[25] Chowdhury, D.R., Iyengar, A.N.S. and Lahiri, S. Gottwald Melborune (01) test for chaos in a plasma, Nonlinear Processes in Geophysics, Vol. 19, pp. 5356, 2012.

[26] Robinson, R.C. An introduction to dynamical systems continuous and discrete, Pearson Prentice Hall, 2004.

[27] Cunha Jr, A.B. Test 01 for chaos, 2017.

[28] Lin, C.T. and Lee, C.S.G. Neural fuzzy systems: a neuro-fuzzy synergism to intelligent systems, Prentice Hall, 1996.

[29] Nauck, D. and Kruse, R. Nefclass - a neuro-fuzzy approach for the classification of data, ACM symposium on applied computing, pp. 461465, 1995.

[30] Lee, Y.K., Kim K.J. Effects of Landing Gear Nonlinearities on Ground Resonance of Helicopter, 14th International Congress of Sound Vibration, 2007.

[31] Gottwald, G. and Melbourne, I. On the implementation of the 0-1 test for chaos, SIAM Journal on Applied Dynamical Systems, Vol. 1, No. 8, pp. 129-145, 2009.

[32] Romero, L.F.S. Classificação de Previsibilidade do Modelo Global do CPTEC Utilizando Breeding e Inteligência Computacional, Dissertação de Mestrado, Instituto Nacional de Pesquisas Espaciais (INPE), São José dos Campos, 2017.